Front. Phys. 10, 107301 (2015)
DOI 10.1007/s11467-015-0468-y

RESEARCH ARTICLE

First-principle study on the optical response of phosphorene

Jia-He Lin[1], **Hong Zhang**[1,2,†], **Xin-Lu Cheng**[2]

[1] *College of Physical Science and Technology, Sichuan University, Chengdu 610065, China*
[2] *Key Laboratory of High Energy Density Physics and Technology of Ministry of Education, Sichuan University, Chengdu 610065, China*
Corresponding author. E-mail: †*hongzhang@scu.edu.cn*
Received December 31, 2014; accepted February 27, 2015

The optical response of phosphorene nanostructures was studied using time-dependent density functional theory (TDDFT). Compared with the absorption spectrum of graphene, that of the phosphorene nanostructure exhibits high absorbance in the ultraviolet region, which indicates a high light absorptivity. In a low-energy resonance zone, a spectral band extends to the entire near-infrared regions. When the impulse excitation polarizes in the armchair-edge direction, the low-energy plasmon in a few-layer phosphorene nanostructure shows an apparent long-range charge-transfer excitation but is significantly less pronounced along the zigzag-edge direction. The edge configuration significantly affects the absorption spectrum of monolayer phosphorene nanostructures. The armchair-edge and the zigzag-edge serve different functions in the absorption spectrum. Moreover, the absorption spectrum of the few-layer phosphorene nanostructure changes with the number of layers when the impulse excitation polarizes in the armchair-edge direction. In addition, the change in the low-energy resonance zone is significantly different from that in the high-energy resonance zone.

Keywords phosphorene nanostructures

PACS numbers 73.20.Mf, 73.21.-b

Frontiers of Physics

1 Introduction

Functional two-dimensional (2D) semiconductors have motivated intensive research, both theoretical and experimental, in recent decades. Since the 1960s, physicists have studied black phosphorus, a layered material with a high carrier mobility and a fundamental band gap. However, only in 2013 did researchers try to isolate phosphorene, a monolayer of black phosphorus analogous to graphene and monolayer MoS_2 [1–4]. Graphene can replace noble metals in applications for transmitting optical signals because of its π plasmons, which have a relatively long propagation length and do not easily decay [5–9]. However, the absence of a band gap in graphene severely limits its application to nanotransistors, and its low light absorptivity (2.3% in monolayer graphene) limits its application to solar cells [10–13].

Monolayer MoS_2, on the other hand, has a direct band gap of ∼1.8 eV [14, 15]. N-type transistors based on monolayer MoS_2 demonstrate good performance with a high I_{on}/I_{off} ratio of ∼108, a high drain current of up to several hundred mA/mm, and a subthreshold swing down to 74 mV/dec [3,4, 16–18]. However, some recent experiments suggest mobility values that are excessively high for low-power integrated systems, thus limiting the wide application of monolayer MoS_2 in electronics [19, 20].

Physicists have also studied silicene (made from silicon) and germanene (made from germanium), and have attempted to produce stanene (a single layer of tin). Whereas the first two do not possess a natural band gap, stanene is yet to be produced. A problem in creating these single-layer materials is their instability due to reaction with air [21, 22].

A few-layer assembly of even monolayers of phosphorene was recently fabricated successfully [23–25]. Phosphorus atoms are arranged hexagonally and form a slightly puckered surface. However, phosphorene is stable in air. Its edge structure displays both zigzag-edge and armchair-edge characteristics. Similar to graphite, black phosphorus (the bulk counterpart of phosphorene) is also a layered material with weak interlayer van der Waals (vdW) interactions [24].

Phosphorene exhibits a finite and direct band gap within a wide energy range. The sample mobility of

black-phosphorus field-effect transistors is the highest at ~1000 cm^2/Vs, obtained at a thickness of ~10 nm [23]. Considerable attention has been devoted to the special band gap and electric field effect of few-layer phosphorene, but its optical response also deserves consideration. Power conversion efficiency is predicted to reach 16%–18% with bilayer phosphorene; these values are higher than the reported efficiencies of state-of-the-art trilayer graphene/transition-metal dichalcogenide solar cells [26].

A study has shown that armchair phosphorene nanoribbons exhibit an optically active direct band gap, whereas the optical transitions of zigzag phosphorene nanoribbons are inactive around the band gap because of symmetry-forbidden transitions. Results show that phosphorene can exhibit an excellent photoluminescence efficiency [27].

An experiment on few-layer black phosphorus revealed a response to excitation wavelengths from the visible region up to the near-infrared region, which may have important applications in optical sensors [28]. In that study, the influences of different atomic structures of phosphorene were not considered systematically. Research on the influence of different edge states and layers is helpful to understand the optical response of phosphorene nanostructures.

In this study, we present first-principles calculations of the optical response of phosphorene nanostructures. All calculations were based on the real-space time-dependent density functional theory (TDDFT) method. Fischer *et al.* [29] demonstrated that the potential-energy surfaces and nonadiabatic transition probabilities agree semiquantitatively for three different systems: an organic chromophore ligating a transition metal, a quantum dot, and a small molecule. TDDFT successfully predicted the collective excitation of the electrons in graphene. Marinopoulos *et al.* investigated the anisotropic dielectric response of graphite using TDDFT. They found that, for in-plane polarization, local-field effects are infinitesimally small, and both plasmon positions and line shapes are consistent with experiment. They also investigated the optical and loss spectra of carbon nanotubes using TDDFT. The calculated optical spectra are consistent with experiment, in terms of the absolute peak positions and anisotropy effects [30–33]. Mowbray *et al.* [34] described the loss function for periodic graphene through the time-dependent linear response within the random-phase approximation (TDDFT-RPA).

We mainly investigated plasmon excitation in the direction parallel to the plane of the phosphorene nanostructure. Hydrogen atoms were used to passivate the dangling σ bonds at the edges. Geometries of phosphorene nanostructures exhibited different rectangular shapes. The effect of different geometries and sizes on the collective excitation was also studied. The effects of the edge configuration and of confinement in all dimensions are discussed. The influence of different numbers of phosphorene layers, from one to three, is also reviewed.

2 Computational methods

2.1 Photoabsorption spectra from TDDFT

Given that photoabsorption is a time-dependent process, TDDFT can in principle be employed to calculate the photoabsorption spectrum of the system. This spectrum can be calculated using TDDFT, either by propagating the time-dependent Kohn–Sham equations in real time [35] or by calculating the linear response of the electrons to the external potential in the frequency domain, as demonstrated by Casida [36]. The first method was used in the present study. The initial state at time $t = 0$ was perturbed with a time-dependent potential [37],

$$v(r,t) = -hk_0x_\nu\delta(t)/(2\pi), \tag{1}$$

where $x_\nu = x, y, z$, and k_0 is the momentum transferred to the system. To ensure that the system has a linear response, the momentum must be very small. Thus, all frequencies of the system are excited with equal weight. We define $\varphi_i(r)$ as the ground-state Kohn–Sham wave functions of the system. The initial state for the time evolution at $r = 0$ is

$$\psi_i(r,0) = \exp(\mathrm{i}k_0x_\nu)\varphi_i(r). \tag{2}$$

The Kohn–Sham wave functions are propagated over a finite but long time period. The information on the excitations is deduced from the dipole-strength function $S(\omega)$. This function measures how strongly a given frequency ω excites the system, and can be written as [35, 37]

$$S(\omega) = \frac{4m_e\omega}{he^2}\Im\sum_\nu \alpha_{\nu\nu}(\omega), \tag{3}$$

where the dynamic polarizability $\alpha_{\mu\nu}(\omega)$ is

$$\alpha_{\mu\nu}(\omega) = \frac{2\pi e^2}{hk_0}\int \mathrm{d}r x_\nu \delta n(r,\omega). \tag{4}$$

2.2 Computational details

All calculations were performed using the real-space and real-time TDDFT code OCTOPUS [30]. Phosphorus and hydrogen atoms were described by the Hartwigsen–Goedecker–Hutter pseudopotentials [38]. The general-

ized gradient approximation (GGA) with the Perdew–Burke–Ernzerhof functional for the exchange-correlation was used in both the ground-state and excited-state calculations [39, 40]. The simulation zone was defined by defining a sphere around each atom with a radius of 6 Å and a uniform mesh grid of 0.3 Å. In the real-time propagation, the excitation spectrum was extracted by a Fourier transform of the dipole strength induced by an impulse excitation [35]. Simultaneously, the response to the particular polarization could be obtained. This scheme has previously been used to predict collective excitations of small sodium clusters with linear structures [33]. In real-time propagation, the time step is $\Delta t = 0.005\ \hbar/\text{eV}$ [41].

3 Results and discussion

We used Cartesian coordinates and atoms fixed in the X–Y plane. For the rectangular monolayer phosphorene nanostructures, the armchair-edge was parallel to the X-axis, whereas the zigzag-edge was perpendicular. In the two-layer phosphorene nanostructure, the edge of the puckered hexagon of the top layer was located in the center of the puckered hexagon of the bottom layer, as shown in Fig. 1(a). In the three-layer phosphorene nanostructure, the edges of the puckered hexagon of the bottom layer and the top layer were located in the center of the puckered hexagon of the middle layer, and the top layer can be seen as the bottom layer after vertical transition, as shown in Fig. 1(b). Moreover, the interlayer spacing is approximately 5 Å, as shown in Fig. 1(c). We investigated mainly plasmon excitations in the direction parallel to the plane of the phosphorene nanostructure [23].

3.1 Plasmons in rectangular monolayer phosphorene nanostructures

Figures 2(a) and (b) show the dipole response (optical absorption) of the rectangular monolayer phosphorene nanostructures to an impulse excitation polarized, respectively, along the X- and Y-axes. The low-energy regimes are magnified in (c) and (d), respectively. A, B, and C identify the three different monolayer phosphorene nanostructures. The width of nanostructure C is greater than that of A along the zigzag-edge direction, whereas the width of the B along the armchair-edge direction is greater than that of A. Each phosphorus atom contributes three valence electrons to form a σ bond with three neighboring atoms in phosphorene. Given the weak σ bond, the optical excitation produced when the photon energy is greater than the energy gap results in the formation of an electron and a hole in the phosphorene.

Compared with the absorption spectrum of graphene [41], that of the monolayer phosphorene nanostructure exhibits greater absorbance in the ultraviolet region. This observation suggests that monolayer phosphorene absorbs light strongly, suggesting a potential application to fabricating thin-film solar cells [26] and photoelectric converters. Comparing Fig. 2(a) with Fig. 2(b), we find that the absorption peak (at approximately 9 eV) along the zigzag-edge direction is higher and narrower than that along the armchair-edge direction. This difference can be attributed to the fact that the phosphorene nanostucture exhibits metallic behavior along the zigzag-edge direction and semiconductor behavior along the armchair-edge direction [43]. In addition, when the edge widths of monolayer phosphorene nanostructures are broadened along the polarization direction, the spectrum band becomes red-shifted. This phenomenon reflects the fact that the band gap of monolayer phosphorene nanostructures decreases with increasing width. Compared with the direction along the zigzag edge, the spectrum band is red-shifted along the armchair-edge direction owing to different potential distributions.

Comparing Fig. 2(c) with Fig. 2(d), optical transitions are active for the first pair of valence and conduction bands (approximately 1eV) along the armchair-edge direction in the low-energy resonance zone. This phenomenon is similar to experimental observations [27]. Meanwhile, the value is nearly zero between 0 and 2 eV along the zigzag-edge direction, similar to what has been observed in silicon nanowires. This result can be attributed to the folding of the band, which makes the material suitable for applications associated with

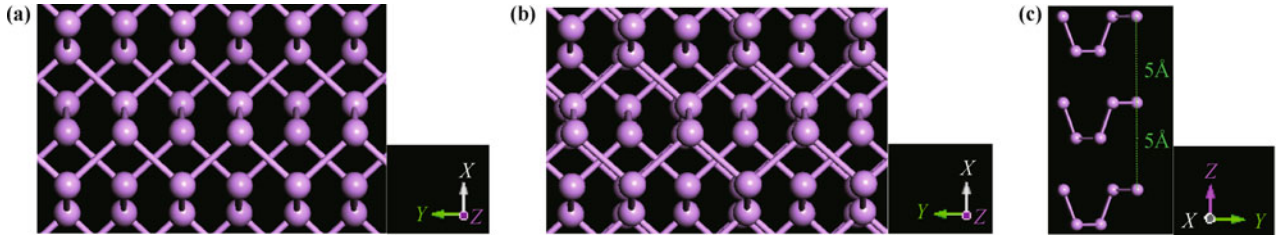

Fig. 1 Stacking structures of **(a)** two-layer and **(b)** three-layer phosphorene. **(c)** Interlayer spacing of few-layer phosphorene.

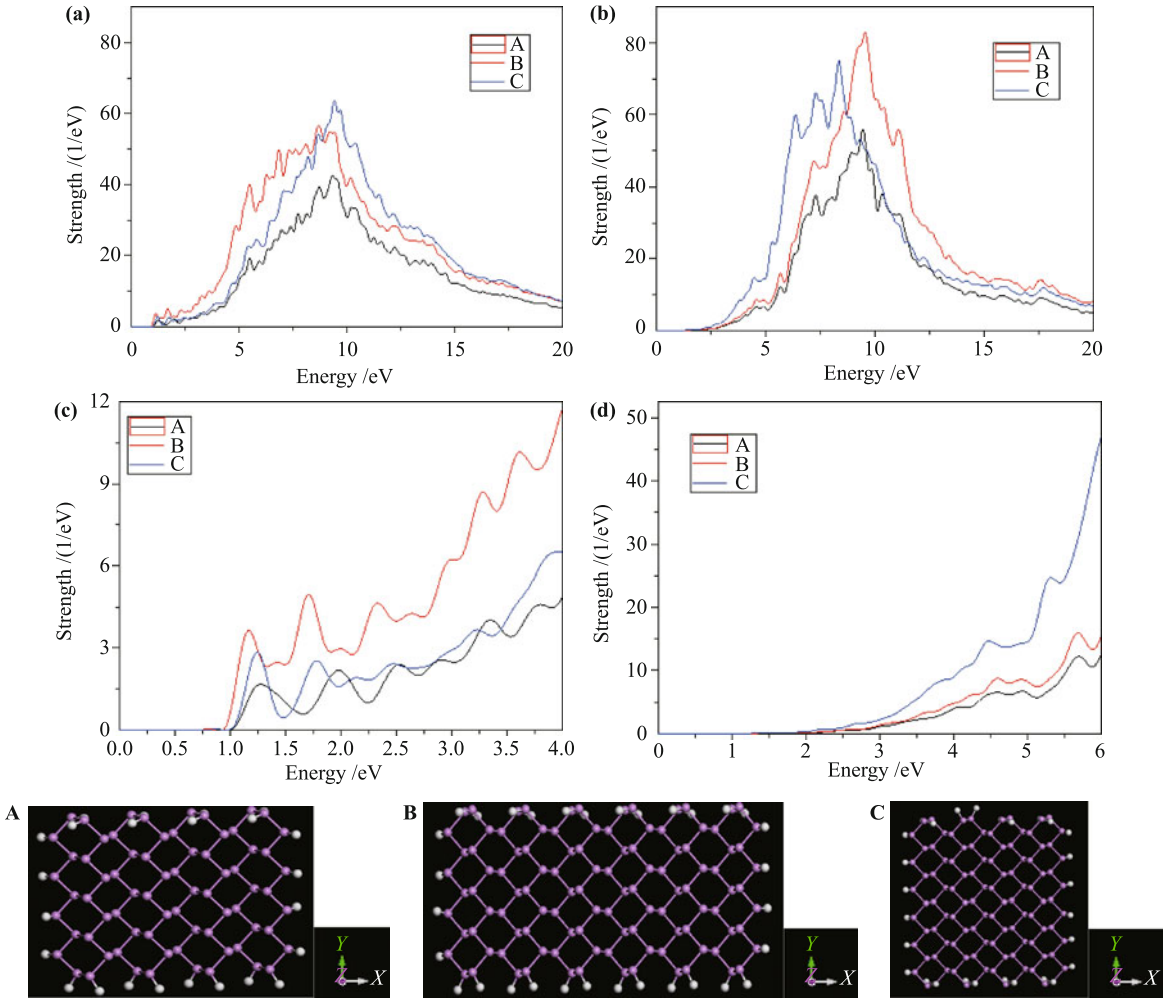

Fig. 2 Dipole response (optical absorption) of the rectangular monolayer phosphorene nanostructures to an impulse excitation polarized in the X-axis **(a)** and Y-axis **(b)** directions. **(c)** is the low-energy part of (a), whereas **(d)** is the low-energy part of (b). **A**, **B**, and **C** are the different structures, as shown in the schematic diagrams of the monolayer phosphorene nanostructures.

long-lifetime dark excitation [42–44]. Interestingly, when the impulse excitation polarizes in the zigzag-edge direction of the C phosphorene nanostructure, which is the widest along this direction, the absorption peak near 1 eV is stronger than that of the A phosphorene nanostructure. For the B phosphorene nanostructure, which is the widest along the armchair-edge direction, the strength of plasmon resonances near 1 eV is stronger than that of the A phosphorene nanostructure. On the other hand, the absorption peak is clearly red-shifted owing to the decrease in energy gap with increasing width along the armchair-edge direction. For the impulse excitation polarized in a zigzag-edge direction, the width of the nanostructure along the X-axis direction influences the absorption spectrum negligibly. In contrast, the width along the Y-axis direction influences the strength and position in the absorption spectrum when C is compared with A. To elucidate the mechanism behind the resonance phenomena, the induced charge response was analyzed in real-time propagation.

We mainly analyzed the induced charge response of the low-energy resonance zone. Figure 3 shows the planar Fourier transform of the induced density, obtained from temporal evolution. The induced density plane is parallel to the plane of the monolayer phosphorene nanostructure. The induced density plane is located in the middle of the pucker because the thickness of the monolayer phosphorene nanostructure is approximately 1.8 Å, and the vertical distance between the phosphorene nanostructure plane and this induced density plane is 0.9 Å [41]. Figure 3 shows a commonly observed feature: the induced charge of most resonance points is distributed in the boundary region because of the spatial separation of electrons and holes in phosphorene [45]. We argue that

the low-energy plasmon is a long-range charge transfer excitation that can be attributed to the electronic motion along the direction in which the electrons move further. However, in the low-energy region, the induced charge distribution also has some different characteristics that can be attributed to the impulse excitation polarized in different directions and for different widths of nanostructures. First, for the impulse excitation polarized in the armchair-edge direction, the induced charge exhibits bilateral symmetry about the electrons and holes, as shown in Figs. 3(a), (c), and (e). Meanwhile, longitudinal symmetry is significantly less pronounced when the impulse excitation polarizes in the zigzag-edge direction, as shown in Figs. 3(b), (d), and (f). The main reason for

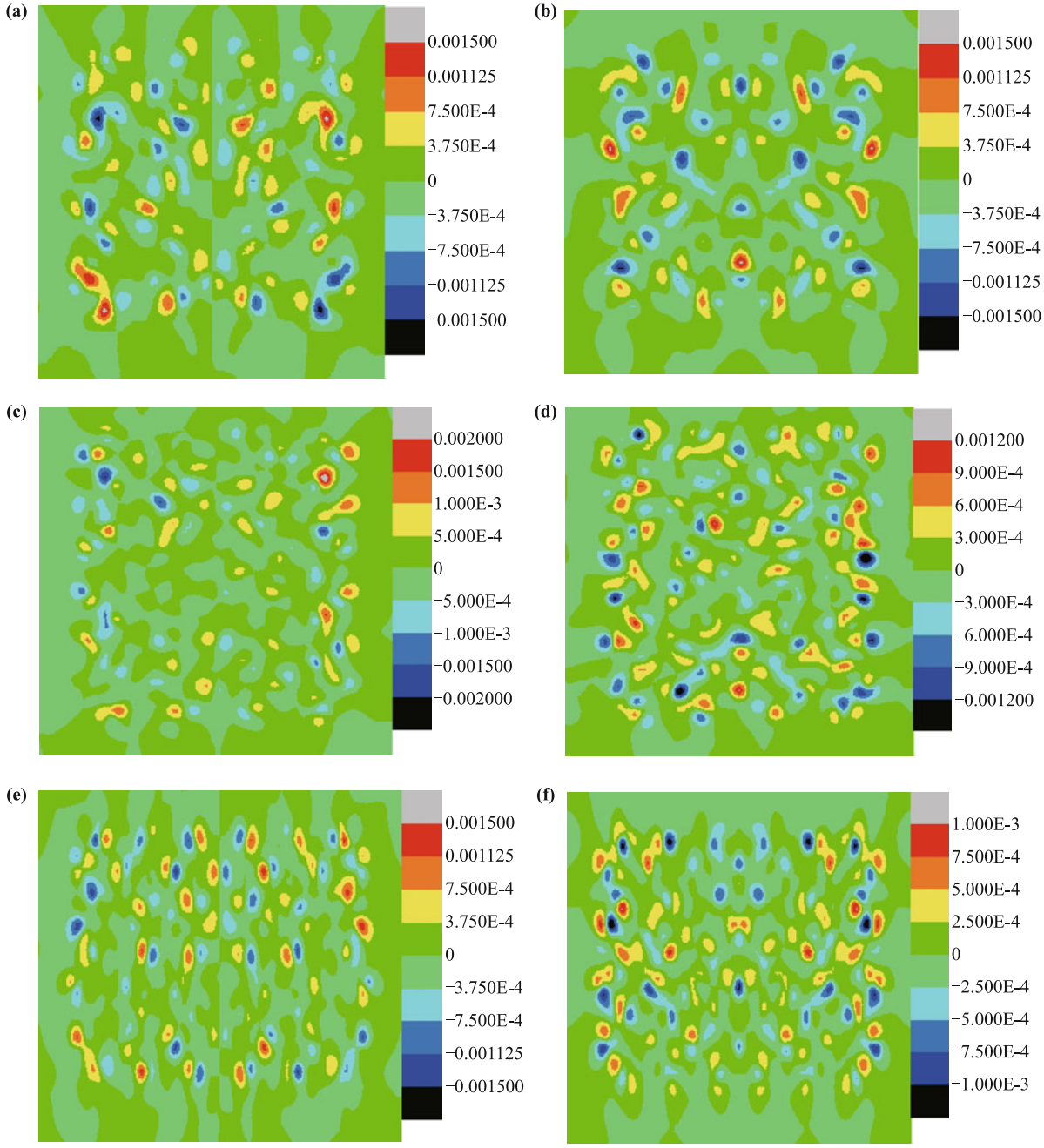

Fig. 3 Fourier transform of the induced charge density for phosphorene nanostructures A, C, and B. For (a), (c), and (e), the polarization direction is along the armchair-edge at the energy resonance points 1.28 eV **(a)** of A, 1.25 eV **(c)** of C, and 1.17 eV **(e)** of B, respectively. For (b), (d), and (f), the polarization direction is along the zigzag-edge at the energy resonance points 5.70 eV **(b)** of A, 5.33 eV **(d)** of C, and 5.59 eV **(f)** of B, respectively.

this difference is that the curvature of the isopotential surfaces is anisotropic in the phosphorene nanostructures [41]. For this reason, no plasmon resonances are observed near 1 eV when the impulse excitation polarizes in the zigzag-edge direction. Comparing Fig. 3(a) with Fig. 3(c), the density of the electrons and holes is stronger and more focused when the width becomes larger along the zigzag-edge. This phenomenon suggests that the C phosphorene nanostructure has a relatively strong absorption peak near 1.25 eV. In Fig. 3(e), the induced charge of the B phosphorene nanostructure is rich but relatively decentralized, which reflects the characteristic of its absorption peak near 1.17 eV. The above discussions focused on the main absorption peak in the low-energy region, but different induced charge distributions are observed for other peaks.

3.2 Plasmons in few-layer phosphorene nanostructures

Figures 4(a) and (c) show the optical absorption of the few-layer phosphorene nanostructure to an impulse excitation polarized in the X- and Y-directions. Figure 4(b) is the low-energy part of (a), whereas (d) is the low-energy part of (c). A, D, and E correspond to the monolayer, bilayer, and trilayer phosphorene nanostructures, respectively. The optical absorption spectra of the bilayer and trilayer phosphorene nanostructures are generally similar to that of the monolayer phosphorene nanostructure. Some differences are observed as the number of layers increases in few-layer phosphorene nanostructures. Figures 4(a) and (c) reveal that bilayer and trilayer phosphorene also have high absorptivity in the ultraviolet region, and the absorption value of phosphorene nanostructures increases with the number of layers. This result shows that light absorptivity can be improved by appropriately increasing the number of layers in few-layer phosphorene nanostructures. However, the absorption spectrum of the bilayer and trilayer phosphorene are weakened comparing to the twofold and threefold intensity of the spectrum for monolayer phosphorene. This phenomenon can be attributed to the fact that the light absorption of phosphorene produces excited charge transfers and forms an electric field that can impair the transfer of excited charge in other layers. In the low-energy zone, the absorption spectrum is red-shifted with the increasing number of layers and the corresponding optical band gaps are 1.04 eV (monolayer), 0.6 eV (bilayer) and 0.31 eV (trilayer). This phenomenon results from the decrease in energy gap with increasing number of layers. Our results are similar to the calculation by GW-BSE [45]. The optical absorption edges were found to start approximately from the band gap [24]. Therefore, the optical absorption edge may be used to tune the band gap in phosphorene nanostructures [28]. Interestingly, the strength of the first absorption peak decreases with increasing number of layers.

Figures 4(e) and (f) show the Fourier transform of the induced charge density for the middle layer of phosphorene nanostructure E. In Fig. 4(e), the polarization direction is along the armchair edge at the energy resonance point 0.93 eV. In Fig. 4(f), the polarization direction is along the zigzag edge at the energy resonance point 4.87 eV. The induced density plane is located in the middle of the pucker. For the impulse excitation polarized in the armchair-edge direction, the induced charge exhibits bilateral symmetry with respect to the electrons and holes, as shown in Fig. 4(e). The longitudinal symmetry is significantly less pronounced when the impulse excitation polarizes in the zigzag-edge direction, as shown in Fig. 4(f). This finding suggests that the low-energy plasmon in the few-layer phosphorene nanostructures should be a long-range charge transfer excitation along the armchair-edge direction. Compared with the induced charge density shown in Fig. 3, that for the middle layer of phosphorene nanostructure E is significantly weaker. This finding reflects the fact that the first absorption peak weakens with increasing number of layers.

4 Conclusion

Using TDDFT, we conducted a systematic study of the collective excitations of a monolayer phosphorene nanostructure with rectangular geometry. We focused on the optical absorption of the few-layer phosphorene nanostructures with the impulse excitation polarized in the armchair-edge direction. Based on these calculations, the following conclusions can be drawn:

For monolayer phosphorene nanostructures, the absorption spectrum of the phosphorene nanostructure is strong in the ultraviolet region compared with that of graphene. This finding suggests that monolayer phosphorene has a high light absorptivity, suggesting potential applications to thin-film solar cells. In the low-energy resonance zone, the spectral band extends to the entire near-infrared region, as observed experimentally. The edge configuration has a significant effect on the absorption spectrum of monolayer phosphorene nanostructures. The phosphorene nanostuctures exhibit metallic behavior along the zigzag-edge direction but semiconductor behavior along the armchair-edge direction. In the low-energy resonance zone, the spectrum is red-shifted with increasing length of the monolayer phosphorene nanostructure in the absorption direction. This phenomenon

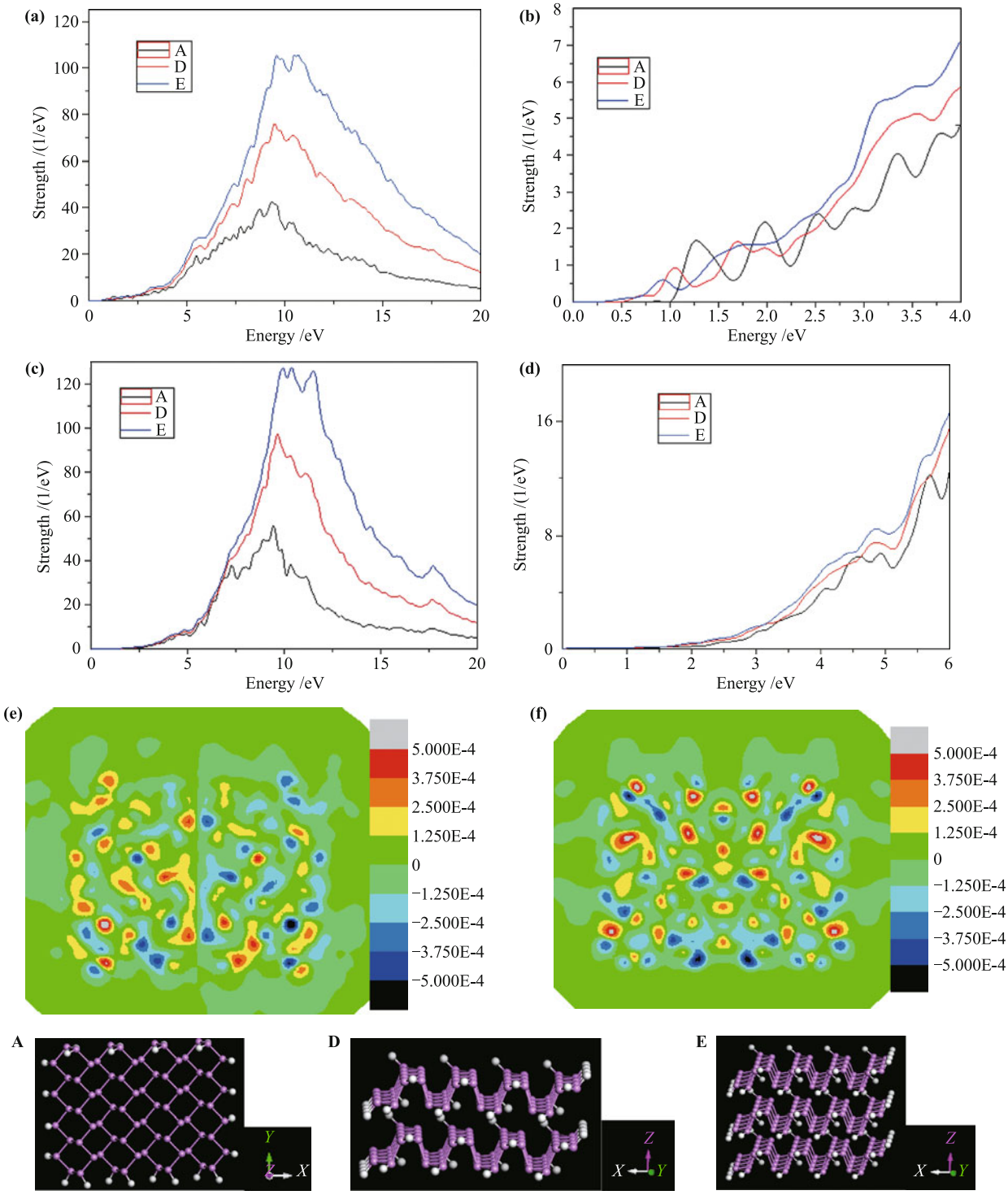

Fig. 4 Optical absorption of the few-layer phosphorene nanostructures to an impulse excitation polarized on the X-axis **(a)** direction. **(b)** is the low-energy part of (a). Optical absorption of the few-layer phosphorene nanostructures to an in impulse excitation polarized on the Y-axis **(c)** direction. **(d)** is the low-energy part of the (c). **(e)** and**(f)** show the Fourier transform of the induced charge density for the middle layer of phosphorene nanostructure E. For (e), the polarization direction is along the armchair-edge at the energy resonance point 0.93 eV. For (f), the polarization direction is along the zigzag-edge at the energy resonance point 4.87 eV. **A**, **D**, and **E** correspond to the monolayer phosphorene nanostructure, the bilayer phosphorene nanostructure, and the trilayer nanostructure, respectively. A, D, and E are the schematic diagrams of the few-layer phosphorene nanostructures.

shows that the low-energy plasmon resonance mode is a long-range charge-transfer excitation and that the band gap decreases with increasing length in the absorption direction. The induced charge of most low-energy resonance points is distributed in the boundary region. This phenomenon is similar to that observed in the graphene nanostructure. For the impulse excitation polarized in the armchair-edge direction, the induced charge exhibits bilateral symmetry with respect to the electrons and holes. Meanwhile, longitudinal symmetry is significantly less pronounced when the impulse excitation polarizes in the zigzag-edge direction.

In few-layer phosphorene nanostructures, the number of layers is a crucial determinant of the absorption spectrum. The absorption value of phosphorene nanostructures increases with increasing number of layers. The light absorption of phosphorene can produce excited charge transfers and form an electric field that may hinder the transfer of excited charge in other layers. When the impulse excitation is polarized in the armchair-edge direction, the optical absorption edges begin near the band gap. Therefore, the optical absorption edge may be used to tune the band gap. Owing to their spatial anisotropy, once the sample orientation is determined, it is much easier to fabricate electrodes or gates utilizing the highest-mobility direction of a few-layer phosphorene sample in an FET-type device [46]. Furthermore, because of the selection rules associated with the symmetries of phosphorene, phosphorene is a natural optical linear polarizer that can be used in liquid-crystal displays, three-dimensional visualization techniques, (bio)-dermatology, and in optical quantum computers [45, 47, 48–52]. Optical-absorption spectra of phosphorene are suitable for a wide range of applications such as infrared sensors.

Acknowledgements We acknowledge the financial support from the National Natural Science Foundation of China (Grant Nos. 11474207 and 11374217).

References

1. K. S. Novoselov, A. K. Geim, S. Morozov, D. Jiang, M. Katsnelson, I. Grigorieva, S. V. Dubonos, and A. Firsov, Two-dimensional gas of massless Dirac fermions in graphene, *Nature* 438(7065), 197 (2005)
2. Y. Zhang, Y. W. Tan, H. L. Stormer, and P. Kim, Experimental observation of the quantum Hall effect and Berry's phase in graphene, *Nature* 438(7065), 201 (2005)
3. B. Radisavljevic, A. Radenovic, J. Brivio, V. Giacometti, and A. Kis, Single-layer MoS_2 transistors, *Nat. Nanotechnol.* 6(3), 147 (2011)
4. H. Fang, M. Tosun, G. Seol, T. C. Chang, K. Takei, and A. Javey, Degenerate n-doping of few-layer transition metal dichalcogenides by potassium, *Nano Lett.* 13(5), 1991 (2013)
5. M. Jablan, H. Buljan, and M. Soljacic, Plasmonics in graphene at infrared frequencies, *Phys. Rev. B* 80(24), 245435 (2009)
6. F. H. L. Koppens, D. E. Chang, and F. J. G. de Abajo, Graphene plasmonics: A platform for strong light–matter interactions, *Nano Lett.* 11(8), 3370 (2011)
7. H. A. Atwater, The promise of plasmonics, *Sci. Am.* 296(4), 56 (2007)
8. E. Ozbay, Plasmonics: Merging photonics and electronics at nanoscale dimensions, *Science* 311(5758), 189 (2006)
9. A. Boltasseva and H. A. Atwater, Low-loss plasmonic metamaterials, *Science* 331(6015), 290 (2011)
10. L. Liao, Y. C. Lin, M. Bao, R. Cheng, J. Bai, Y. Liu, Y. Qu, K. L. Wang, Y. Huang, and X. Duan, High-speed graphene transistors with a self-aligned nanowire gate, *Nature* 467(7313), 305 (2010)
11. F. Schwierz, Graphene transistors, *Nat. Nanotechnol.* 5(7), 487 (2010)
12. Y. Wu, Y. Lin, A. A. Bol, K. A. Jenkins, F. Xia, D. B. Farmer, Y. Zhu, and P. Avouris, High-frequency, scaled graphene transistors on diamond-like carbon, *Nature* 472(7341), 74 (2011)
13. Y. L. Chen, X. B. Feng, and D. D. Hou, Optical absorptions in monolayer and bilayer grapheme, *Acta Phys. Sin.* 62(18), 187301 (2013)
14. K. F. Mak, C. Lee, J. Hone, J. Shan, and T. F. Heinz, Atomically thin MoS_2: A new direct-gap semiconductor, *Phys. Rev. Lett.* 105(13), 136805 (2010)
15. A. Splendiani, L. Sun, Y. B. Zhang, T. S. Li, J. Kim, C. Y. Chim, G. Galli, and F. Wang, Emerging photoluminescence in monolayer MoS_2, *Nano Lett.* 10(4), 1271 (2010)
16. H. Liu and P. D. Ye, MoS_2 dual-gate MOSFET with atomic-layer-deposited Al_2O_3 as top-gate dielectric, *IEEE Electron Device Lett.* 33(4), 546 (2012)
17. H. Liu, A. T. Neal, and P. D. Ye, Channel length scaling of MoS_2 MOSFETs, *ACS Nano* 6(10), 8563 (2012)
18. Y. Yoon, K. Ganapathi, and S. Salahuddin, How good can monolayer MoS_2 transistors be? *Nano Lett.* 11(9), 3768 (2011)
19. B. Radisavljevic, M. B. Whitwick, and A. Kis, Integrated circuits and logic operations based on single-layer MoS_2, *ACS Nano* 5(12), 9934 (2011)
20. H. Wang, L. Yu, Y. H. Lee, Y. Shi, A. Hsu, M. L. Chin, L. J. Li, M. Dubey, J. Kong, and T. Palacios, Integrated circuits based on bilayer Mo_2 transistors, *Nano Lett.* 12(9), 4674 (2012)
21. E. S. Reich, Phosphorene excites materials scientists, *Nature* 506(7486), 19 (2014)
22. Y. Xu, B. Yan, H.J. Zhang, J. Wang, G. Xu, P. Tang, W. Duan, and S.C. Zhang, Large-gap quantum spin Hall insulators in tin films, *Phys. Rev. Lett.* 111(13), 136804 (2013)

23. L. Li, Y. J. Yu, G. J. Ye, Q. Q. Ge, X. D. Ou, Hua Wu, D. L. Feng, X. H. Chen, and Y. Zhang, Black phosphorus field-effect transistors, *Nat. Nanotechnol.* 2014, 9(5), 372
24. H. Liu, A. T. Neal, Z. Zhu, Z. Luo, X. F. Xu, D. Tomanek, and P. D. Ye, Phosphorene: An unexplored 2D semiconductor with a high hole mobility, *ACS Nano* 8(4), 4033 (2014)
25. E. S. Reich, Phosphorene excites materials scientists, *Nature* 506(7486), 19 (2014)
26. J. Dai and X. C. Zeng, Bilayer phosphorene: Effect of stacking order on bandgap and its potential applications in thin-film solar cells, *J. Phys. Chem. Lett.* 5(7), 1289 (2014)
27. M. Buscema, D. J. Groenendijk, S. I. Blanter, G. A. Steele, H. S. J. van der Zant, and A. Castellanos-Gomez, Fast and broadband photoresponse of few-layer black phosphorus field-effect transistors, *Nano Lett.* 14(6), 3347 (2014)
28. V. Tran and L. Yang, Scaling laws for the band gap and optical response of phosphorene nanoribbons, *Phys. Rev. B* 89(24), 245407 (2014)
29. S. A. Fischer, B. F. Habenicht, A. B. Madrid, W. R. Duncan, and O. V. Prezhdo, Regarding the validity of the time-dependent Kohn–Sham approach for electron-nuclear dynamics via trajectory surface hopping, *J. Chem. Phys.* 134(2), 024102 (2011)
30. M. A. L. Marques, A. Castro, G. F. Bertsch, and A. Rubio, Octopus: A first-principles tool for excited electron–ion dynamics, *Comput. Phys. Commun.* 151(1), 60 (2003)
31. A. Rubio, J. A. Alonso, J. M. Lopez, and M. J. Stott, Surface plasmon excitations in C_{60}, $C_{60}K$ and $C_{60}H$ clusters, *Physica B* 183(3), 247 (1993)
32. A. G. Marinopoulos, L. Reining, V. Olevano, A. Rubio, T. Pichler, X. Liu, M. Knupfer, and J. Fink, Anisotropy and interplane interactions in the dielectric response of graphite, *Phys. Rev. Lett.* 89(7), 076402 (2002)
33. A. G. Marinopoulos, L. Reining, A. Rubio, and N. Vast, Optical and loss spectra of carbon nanotubes: Depolarization effects and intertube interactions, *Phys. Rev. Lett.* 91(4), 046402 (2003)
34. K. De Blauwe, D. J. Mowbray, Y. Miyata, P. Ayala, H. Shiozawa, A. Rubio, P. Hoffmann, H. Kataura, and T. Pichler, Combined experimental and ab initio study of the electronic structure of narrow-diameter single-wall carbon nanotubes with predominant (6,4),(6,5) chirality, *Phys. Rev. B* 82(12), 125444 (2010)
35. K. Yabana and G. F. Bertsch, Time-dependent local-density approximation in real time, *Phys. Rev. B* 54(7), 4484 (1996)
36. C. Jamorski, M. E. Casida, and D. R. Salahub, Dynamic polarizabilities and excitation spectra from a molecular implementation of time-dependent density-functional response theory: N_2 as a case study, *J. Chem. Phys.* 104(13), 5134 (1996)
37. J. O. Joswig, L. O. Tunturivuori, and R. M. Nieminenc, Photoabsorption in sodium clusters on the basis of time-dependent density-functional theory, *J. Chem. Phys.* 128(1), 014707 (2008)
38. C. Hartwigsen, S. Goedecker, and J. Hutter, Relativistic separable dual-space Gaussian pseudopotentials from H to Rn, *Phys. Rev. B* 58(7), 3641 (1998)
39. A. Rubio-Ponce, A. Conde-Gallardo, and D. Olguin, First-principles study of anatase and rutile TiO_2 doped with Eu ions: A comparison of GGA and LDA+U calculations, *Phys. Rev. B* 78(3), 0351071 (2008)
40. A. Delin, L. Fast, B. Johansson, O. Eriksson, and J. M. Wills, Cohesive properties of the lanthanides: Effect of generalized gradient corrections and crystal structure, *Phys. Rev. B* 58(8), 4345 (1998)
41. H. Yin and H. Zhang, Plasmons in graphene nanostructures, *J. Appl. Phys.* 111(10), 103502 (2012)
42. J. Guan, Z. Zhu, and D. Tománek, Phase coexistence and metal-insulator transition in few-layer phosphorene: A computational study, *Phys. Rev. Lett.* 113, 046804 (2014)
43. L. Yang, C. D. Spataru, S. G. Louie, and M. Y. Chou, Enhanced electron-hole interaction and optical absorption in a silicon nanowire, *Phys. Rev. B* 75(20), 201304 (2007) (R)
44. M. Reischle, G. J. Beirne, R. Roßbach, M. Jetter, and P. Michler, Influence of the dark exciton state on the optical and quantum optical properties of single quantum dots, *Phys. Rev. Lett.* 101(14), 146402 (2008)
45. V. Tran, R. Soklaski, Y. Liang, and L. Yang, Tunable band gap and anisotropic optical response in few-layer black phosphorus, arXiv: 1402.4192, 2014
46. J. Qiao, X. Kong, Z. X. Hu, F. Yang, and W. Ji, High-mobility transport anisotropy and linear dichroism in few-layer black phosphorus, *Nat. Commun.* 5, 4475 (2014)
47. N. Zeng, X.-Y. Jiang, Q. Gao, Y. He, and H. Ma, Linear polarization difference imaging and its potential applications, *Appl. Opt.* 48(35), 6734 (2009)
48. E. Knill, R. Laflamme, and G. J. Milburn, A scheme for efficient quantum computation with linear optics, *Nature* 409(6816), 46 (2001)
49. N. P. Dasgupta and P. Yang, Semiconductor nanowires for photovoltaic and photoelectrochemical energy conversion, *Front. Phys.* 9(3), 289 (2014)
50. Y. L. Zhao, Y. L. Song, W. G. Song, W. Liang, X. Y. Jiang, Z. Y. Tang, H. X. Xu, Z. X. Wei, Y. Q. Liu, M. H. Liu, L. Jiang, X. H. Bao, L. J. Wan, and C. L. Bai, Progress of nanoscience in China, *Front. Phys.* 9(3), 257 (2014)
51. N. Liu, W. Li, M. Pasta, and Y. Cui, Nanomaterials for electrochemical energy storage, *Front. Phys.* 9(3), 323 (2014)
52. W.-J. Li, D.-X. Yao, and E. W. Carlson, Tunable nano Peltier cooling device from geometric effects using a single graphene nanoribbon, *Front. Phys.* 9(4), 472 (2014)